Three-Dimensional Coronary Artery Microscopy by Intracoronary Optical Frequency Domain Imaging

Guillermo J. Tearney, MD, PHD,*‡¶ Sergio Waxman, MD,§‖ Milen Shishkov, PHD,*†
Benjamin J. Vakoc, PHD,*† Melissa J. Suter, PHD,*† Mark I. Freilich, MBBS,§
Adrien E. Desjardins, PHD,*†¶ Wang-Yul Oh, PHD,*† Lisa A. Bartlett, BS,*†
Mireille Rosenberg, PHD,* Brett E. Bouma, PHD*†¶

Boston, Burlington, and Cambridge, Massachusetts

OBJECTIVES We present the first clinical experience with intracoronary optical frequency domain imaging (OFDI) in human patients.

BACKGROUND Intracoronary optical coherence tomography (OCT) is a catheter-based optical imaging modality that is capable of providing microscopic ($\sim$7-μm axial resolution, $\sim$30-μm transverse resolution), cross-sectional images of the coronary wall. Although the use of OCT has shown substantial promise for imaging coronary microstructure, blood attenuates the OCT signal, necessitating prolonged, proximal occlusion to screen long arterial segments. OFDI is a second-generation form of OCT that is capable of acquiring images at much higher frame rates. The increased speed of OFDI enables rapid, 3-dimensional imaging of long coronary segments after a brief, nonocclusive saline purge.

METHODS Volumetric OFDI images were obtained in 3 patients after intracoronary stent deployment. Imaging was performed in the left anterior descending and right coronary arteries with the use of a nonocclusive saline purge rates ranging from 3 to 4 ml/s and for purge durations of 3 to 4 s. After imaging, the OFDI datasets were segmented using previously documented criteria and volume rendered.

RESULTS Good visualization of the artery wall was obtained in all cases, with clear viewing lengths ranging from 3.0 to 7.0 cm at pullback rates ranging from 5 to 20 mm/s. A diverse range of microscopic features were identified in 2 and 3 dimensions, including thin-capped fibroatheromas, calcium, macrophages, cholesterol crystals, bare stent struts, and stents with neointimal hyperplasia. There were no complications of the OFDI procedure.

CONCLUSIONS Our results demonstrate that OFDI is a viable method for imaging the microstructure of long coronary segments in patients. Given its ability to provide microscopic information in a practical manner, this technology may be useful for studying human coronary pathophysiology in vivo and as a clinical tool for guiding the management of coronary artery disease. (J Am Coll Cardiol Img 2008;1:752–61) © 2008 by the American College of Cardiology Foundation

Optical coherence tomography (OCT) (1–7) is a high-resolution cross-sectional imaging modality that offers the unique possibility of visualizing and quantifying clinically important coronary plaque microstructures, including macrophages (8–10), thin fibrous caps (2,7,11,12), collagen (13–15), thrombus (7,16,17), stent strut apposition (18–21), and stent coverage (4–6,22–30). Although OCT has shown promise

for intracoronary imaging, its clinical applicability has been severely limited by the attenuation of its optical beam by intraluminal blood, which prevents clear visualization of the vessel wall. The 2 most common approaches for displacing blood include: 1) proximal balloon occlusion of the coronary artery followed by saline perfusion; and 2) brief, nonocclusive saline purge through a guiding catheter. Proximal balloon occlusion is undesirable because of its potential to cause myocardial ischemia and vessel injury. Intermittent, nonocclusive saline purges are safe, but the slow image acquisition speed of OCT relative to the duration of clear viewing provided by the saline flush, limits OCT to "snap-shot" imaging at a few discrete locations.

A second-generation OCT technology, termed optical frequency domain imaging (OFDI) (31,32), recently has been developed that solves this problem by imaging at much higher frame rates. Optical frequency domain imaging is the imaging form of optical frequency domain reflectometry, a telecommunications technique that is used to determine fiber fault locations for short- and long-haul optical networks (33). In combination with a short, nonocclusive saline flush and rapid spiral pullback, the higher frame rates generated by OFDI enable imaging of the 3-dimensional (3D) microstructure of long segments of coronary arteries in vivo in swine (31). We report the first clinical experience with intracoronary OFDI.

METHODS

Patients. Patients undergoing percutaneous transluminal coronary intervention for coronary artery disease were enrolled at the Lahey Clinic (Burlington, Massachusetts) from May to September 2007. Partners and Lahey Clinic institutional review boards approved the study. All patients gave informed consent prior to their participation.

The OFDI system and catheter. The OFDI system used in this study (31) provided images at 100 frames/s with a total of 512 radial scans per circular cross-sectional image. Axial resolution was 7 μm in tissue (refractive index n = 1.4), and the signal to noise ratio was 110 dB. All unprocessed data were continuously archived to hard disk drive at a rate of 320 MB/s. During the procedure, every fifth image was reconstructed and displayed in real time at a rate of 20 frames/s. Immediately after the imaging session, all images were reconstructed and stored as a digital movie, which required approximately 15 to 30 s, depending on the number of frames acquired.

The OFDI catheter comprised an optical imaging core within a transparent outer sheath (2.6-F) (3) that incorporated a rapid-exchange guide wire provision. The transverse resolution of the catheter was 30 μm, and the focal distance was 2.5 mm. For rapid spiral imaging, an optical rotary junction rotated the optical imaging core at 100 revolutions per second and pulled the imaging core back at speeds ranging from 5 to 20 mm/s (longitudinal resolutions 50 to 200 μm, respectively) in a manner analogous to that used in rotational intravascular ultrasound (IVUS). The OFDI system, rotary junction, and catheters were fabricated in the Wellman Center for Photomedicine at the Massachusetts General Hospital. The OFDI catheter was assembled under design control guidelines and approved under a U.S. Food and Drug Administration investigational device exemption.

Image acquisition. All patients received intracoronary stents (Cypher, Cordis Corp., Miami Lakes, Florida) as per the standard of care. After intervention, the OFDI catheter was advanced over the 0.014-inch guidewire and through a 7-F guide catheter. The OFDI catheter was then positioned so that its imaging core was distal to the stent. Radiopaque markers on the OFDI catheter sheath and imaging core were used for confirming catheter position during angiography. After catheter placement, a cardiovascular injection system (Avanta, Medrad Warrendale, Pennsylvania) was used to provide a nonocclusive saline (lactated Ringer's solution) flush through the guide catheter at a rate of 2 to 4 ml/s for approximately 3 to 6 s. The maximum saline delivered for any given imaging session was 20 ml. When a blood-free image was observed, the OFDI system operator initiated rapid pullback of the OFDI imaging core by using standalone electronic control of the pullback motor. The pullback and catheter rotation was terminated with the same mechanism when significant intraluminal blood was observed in the OFDI image or when the catheter imaging core entered the guide catheter.

After reconstruction of the digital movie, the catheter imaging core was repositioned, and data acquisition was repeated in each patient several (i.e., 1 to 3) times. Different saline purge parameters (2 to 4 ml/s) and pullback rates (5 to 20 mm/s) were attempted.

Processing of OFDI images and 3D reconstruction. After imaging and reconstruction of the OFDI images, $1024 \times 1024 \times N$ (N = number of frames) pixel data sets were processed offline with the use of ImageJ (34). Image contrast was normalized for each frame of the OFDI movie. Cross-sectional and longitudinal sections were displayed with an inverse gray scale lookup table. Clear visualization lengths were determined by measuring the pullback length over which blood did not significantly alter the signal from the coronary wall. For some patients (OFDI-02 and -03), to remove rotational artifacts caused by cardiac motion, we performed frame-to-frame registration by image registration and rigid body transformation (35). For 3D visualization, the following components of each of the images were manually segmented with previously established OCT plaque and stent characterization criteria (8,9,19,36): 1) artery wall; 2) lipid pool; 3) calcific nodule; and 4) stent. We have previously shown that macrophages can be identified in OCT images by their highly backscattering, punctate appearance, a finding that was validated by comparing OCT data to corresponding histopathology slides stained with CD68 (8). Macrophages were automatically segmented with normalized image intensity metrics on a per-image basis (8) with manual removal of outliers. Three-dimensional median filtering with a $3 \times 3 \times 3$ kernel was conducted for each segmented volume.

After segmentation, the artery data were rendered in color using the following scheme: 1) red = artery wall; 2) yellow = lipid pool; 3) white = calcific nodule; 4) blue = stent; and 5) gray = guide wire. The volumes corresponding to each component were added to generate the final segmented and colored volume data set. Segmented data were imported into a 3D, volume-rendering program (OsiriX 2.75, The OsiriX Foundation, Geneva, Switzerland). Maximum intensity projection and volume rendering techniques were used for visualization and were implemented with several different opacity tables. Cut surfaces and fly-throughs of the rendered data sets also were constructed.

RESULTS

A total of 3 patients (OFDI-01 through OFDI-03) were imaged between May and September 2007.

Baseline characteristics for the patients are presented in Table 1. Imaging was performed successfully in all patients. None of the patients experienced chest pain or electrocardiogram changes during intracoronary OFDI. There were no complications related to the OFDI procedure. A range of saline flow rates (2 to 4 ml/s) and pullback speeds (0.5 to 2.0 cm/s) were used, providing imaging of arterial segments from 3 to 7 cm in length.
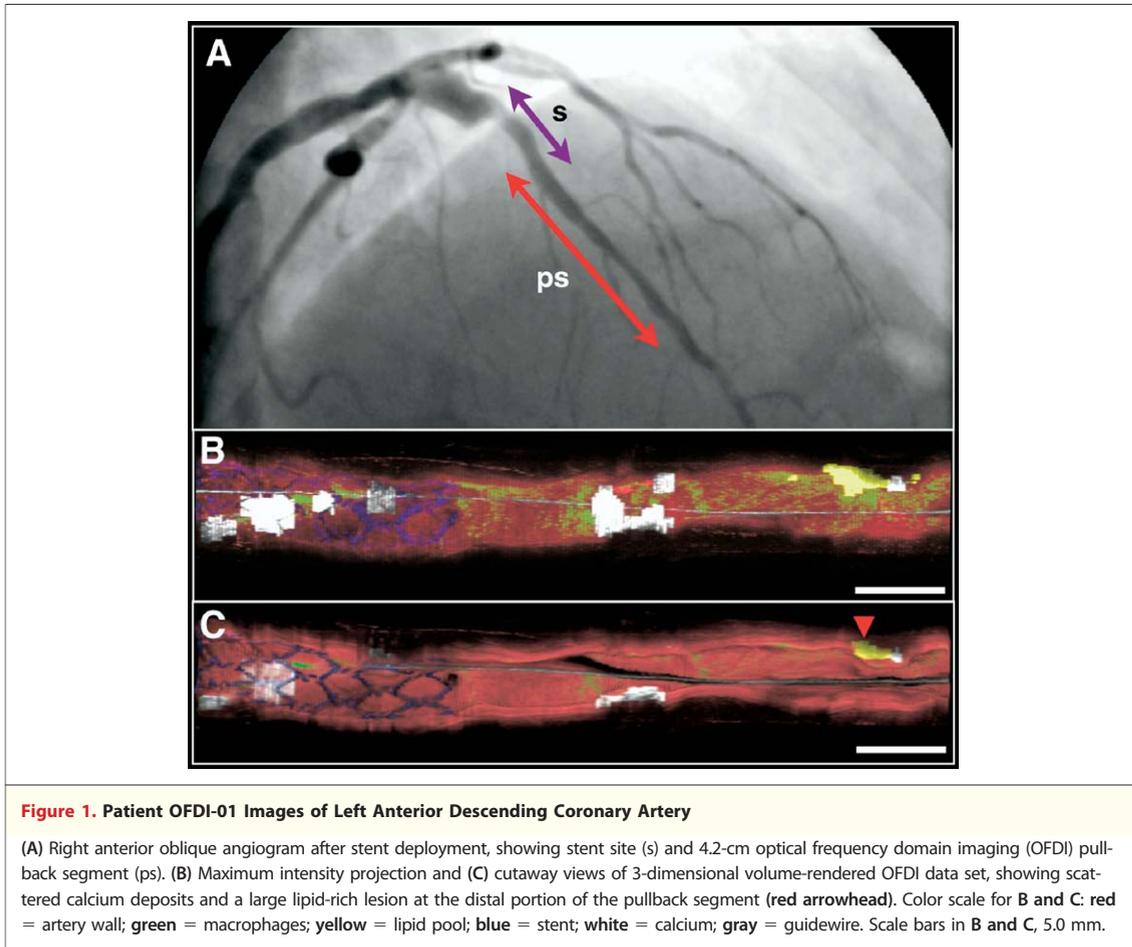
Patient OFDI-01. Patient OFDI-01 had a drug-eluting stent (DES) placed distal to a proximal left anterior descending artery (LAD) aneurysm (Fig. 1A). The OFDI imaging of the proximal LAD originated distal to the stent and terminated within the stent (Fig. 1A). Three-dimensional visualization (Figs. 1B and 1C) of the segmented data set, obtained at a saline purge rate of 3 ml/s and a pullback velocity of 2.0 cm/s, shows the proximal LAD stent (blue) as well as coronary atherosclerosis, including calcific nodules (white), lipid-rich plaque (yellow), and punctate macrophages (green). A longitudinal OFDI section shows a large lipid pool at the distal aspect of the coronary segment (Figs. 2A and 2B). An expanded portion of a cross-sectional image of this lesion (obtained from location denoted by arrow in Fig. 2B) demonstrates that this lipid pool has OFDI features consistent with a thin-capped fibroatheroma (TCFA), including a thin fibrous cap (Fig. 2C, black arrow), and macrophages at the cap–lipid pool junction (Fig. 2C, green arrow). A flap of tissue can be seen over the cap (arrowhead in Fig. 2C), which could represent

Table 1. Patient Characteristics			
	Patient		
Characteristic	**OFDI-01**	**OFDI-02**	**OFDI-03**
Age, yrs	68	52	79
Gender	M	M	M
Family history of CAD	No	Yes	No
Diabetes	No	No	Yes
Hypertension	Yes	Yes	Yes
Hyperlipidemia	Yes	Yes	Yes
BMI, kg/m^2	30.8	37.8	26.2
Total cholesterol, mg/d	159	190	129*
LDL, mg/d	99	95	76*
hsCRP, mg/l	23	<5	<5
Multivessel disease	Yes	Yes†	Yes†
Presentation	SAP	SAP	SAP
Angiographic findings	99% mLAD	99% dRCA	70% mRCA

*Blood taken 6 months before imaging for this patient. †Nonsignificant except for RCA.

BMI = body mass index; CAD = coronary artery disease; dRCA = distal right coronary artery; hsCRP = high-sensitivity C-reactive protein; LDL = low-density lipoprotein; mLAD = middle left anterior descending artery; mRCA = middle right coronary artery; OFDI = optical frequency domain imaging; RCA = right coronary artery; SAP = stable angina pectoris.

Figure 1. Patient OFDI-01 Images of Left Anterior Descending Coronary Artery

(A) Right anterior oblique angiogram after stent deployment, showing stent site (s) and 4.2-cm optical frequency domain imaging (OFDI) pull-back segment (ps). **(B)** Maximum intensity projection and **(C)** cutaway views of 3-dimensional volume-rendered OFDI data set, showing scattered calcium deposits and a large lipid-rich lesion at the distal portion of the pullback segment **(red arrowhead)**. Color scale for **B and C: red** = artery wall; **green** = macrophages; **yellow** = lipid pool; **blue** = stent; **white** = calcium; **gray** = guidewire. Scale bars in **B and C**, 5.0 mm.

disrupted intima or fibrin. In this image, the minimum cap thickness near the shoulder is approximately 60 μm (Fig. 2B arrow; corrected for a refractive index n = 1.4).

Patient OFDI-02. For Patient OFDI-02, imaging was conducted from the distal vessel, across the posterior descending artery, to the proximal segment of the right coronary artery (RCA) (Fig. 3A). Cutaway longitudinal views of volume renderings (Figs. 3B to 3D), acquired at a saline perfusion rate of 3.0 ml/s and a pullback velocity of 2.0 cm/s, show a bare-metal stent (BMS) (Fig. 3C), placed 9 years previously, and a DES, placed immediately before OFDI imaging (Fig. 3D). The entire DES can be visualized, crossing the ostia of the posterior descending artery. Only portions of the BMS can be seen in the cutaway view (Fig. 3C) because of neointimal hyperplasia covering the stent and the transparency chosen for rendering. However, some BMS struts viewed from the luminal aspect appear to have little tissue coverage.

Fly-through views show the BMS and DES in greater detail (Figs. 4A and 4B). Although a portion of the BMS struts (Fig. 4A) have a similar appearance to the DES struts (Fig. 4B), further inspection of cross-sectional OFDI images reveals microscopic distinctions; as opposed to the DES struts (Fig. 4D), the BMS struts (Fig. 4C) appear thicker, have a surface reflectivity that is comparable with that of arterial tissue, and have edges that continuously blend into the luminal surface. These observations are consistent with the presence of a covering over the BMS struts that is thinner than the resolution of the OFDI system.

The angiogram shows minimal luminal stenosis proximal to the DES (yellow arrowhead in Fig. 3A). Volume renderings depict a large lipid pool at this location (see dotted horizontal line in Fig. 3D), which is partially covered by the DES and present at the junction between the DES and artery wall. A fly-through view at this location (Fig. 5A) shows that the lesion is circumferential. A cross-sectional OFDI image (Fig. 5B) at the corresponding site demonstrates that this lesion is a TCFA, with cap thicknesses <65 μm at multiple locations (black arrowheads in Fig. 5B). As in Patient OFDI-01,
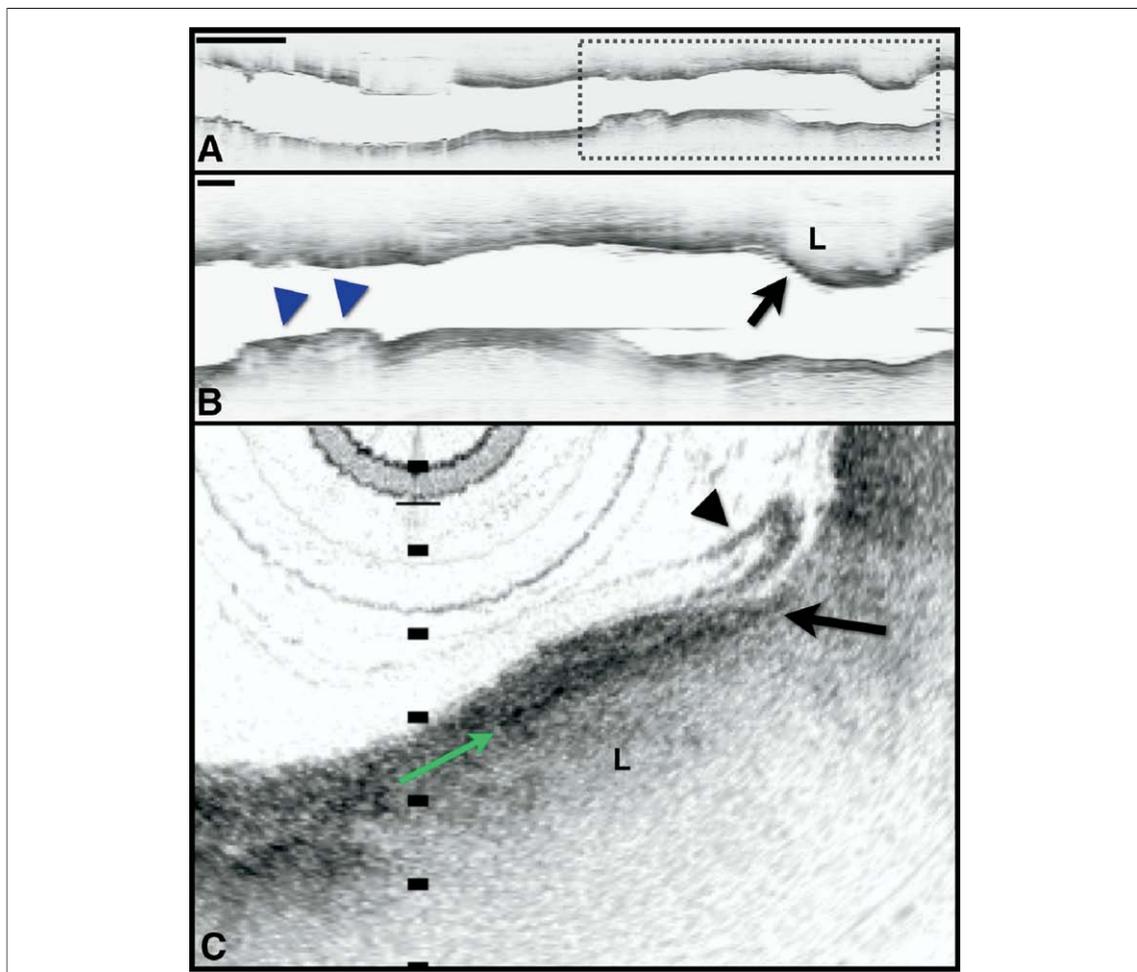
Figure 2. Patient OFDI-01 Longitudinal and Cross-Sectional Images of Left Anterior Descending Artery

(A) Longitudinal optical frequency domain imaging (OFDI) section, corresponding to the cut surface of (Fig. 1C). (B) Expanded view of dotted region in **A**, demonstrating a large calcific nodule (**blue arrowheads**) and a lipid pool with a thin fibrous cap (**black arrow**). (C) Expanded view of an OFDI cross-sectional image obtained at location of the **black arrow in B** and **red arrowhead** in Figure 1C, shows a lipid pool with a thin fibrous cap (**black arrow**) and a dense band of macrophages at the cap–lipid pool interface (**green arrow**). A thin flap of tissue (**black arrowhead**) can be seen over the cap. Scale bar in **A**, 5.0 mm. Scale bar in **B**, 1.0 mm. **Tick marks in C**, 0.25 mm. L = lipid pool.

this TCFA has a cap that contains many macrophages (green arrowheads in Fig. 5B), some of which appear to extend to the luminal surface. Cholesterol crystals can also be identified within the lipid pool (red arrows in Fig. 5B).

Patient OFDI-03. Imaging of Patient OFDI-03 began distal to a mid-RCA DES and terminated within the stent. Figures 6 and 7 depict images obtained with the slowest pullback rate of 5 mm/s and a saline purge rate of 3.0 ml/s. The clear visualization length was 3.0 cm. The stent was deployed over a large calcific nodule, resulting in distortion of the stent struts (Figs. 6B and 6C). Because of the finer longitudinal resolution (50 μm vs. 200 μm), the stent strut microstructure is better appreciated in 3 dimensions and contains fewer discontinuities (Fig. 6B) in comparison with the other

2 cases (Figs. 1 to 5). Improved visualization of the stent struts is also clearly evident in the longitudinal cutaway view (Fig. 7A). A longitudinal reconstruction from this session is shown in Figure 7B, demonstrating a calcific nodule beneath the DES. The longitudinal image's resolution is superior to that obtained with 200-μm longitudinal resolution (Figs. 2A and 2B) and is comparable with that of OFDI image cross sections.

DISCUSSION

Our results demonstrate that all of the coronary microanatomy and pathology previously visualized by OCT, including lipid pools, calcium, macrophages, thin fibrous caps, cholesterol crystals, and thrombus,
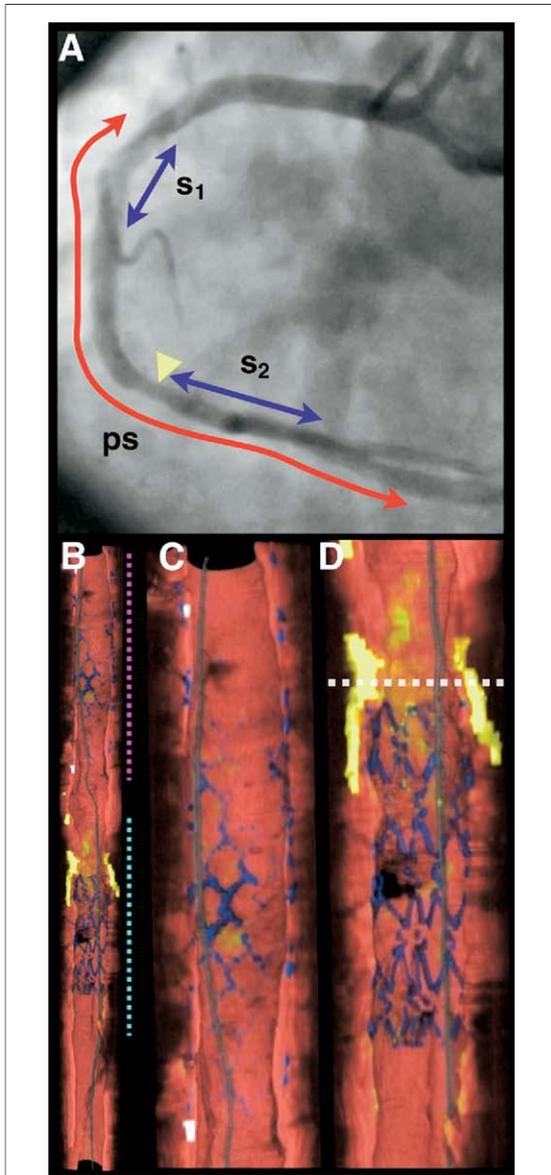
Figure 3. Patient OFDI-02 Images of Right Coronary Artery (Session 2)

(A) Left anterior oblique angiogram after stent deployment, showing previous (s1, BMS) and current (s2, DES) stents and 7.0-cm optical frequency domain imaging (OFDI) pullback segment (ps). (B) Cutaway view of entire 3-dimensional volume rendered OFDI data set (**top** = proximal; **bottom** = distal). (C) Expanded view of segment denoted by **magenta dotted line in B**, showing the BMS. (D) Expanded view of segment denoted by **cyan dotted line in B**, showing the DES. **White dotted line in D** is through a lipid-rich lesion, proximal to the DES. Color scale for **B to D**: **red** = artery wall; **green** = macrophages; **yellow** = lipid pool; **blue** = stent; **white** = calcium; **gray** = guide wire. BMS = bare-metal stent; DES = drug-eluting stent.

hindered the interpretation of data obtained from first-generation OCT systems. In addition to native coronary microscopic pathology, stents and stent neo-intimal hyperplasia were clearly identified in OFDI images from patients in this study. Whether or not OCT or OFDI can be used to visualize single-cell re-endothelialization remains an important subject of future research that will impact its utility for evaluating risk of late stent thrombosis (37).

Study limitations. This was a proof-of-principle study with a limited number of patients, and as such, should be considered preliminary. Nevertheless, the results presented here are promising. The saline perfusion and rapid pullback-imaging scheme worked for all patients, even in cases when it should have been difficult. For example, in Patient OFDI-01, excellent images were obtained even in the presence of a proximal LAD aneurysm and incidental perfusion of the left circumflex coronary artery (LCX) through the left main. To date, we have not imaged the LCX. In other OCT imaging studies, we did not find differences between clear imaging durations for the 3 main coronary arteries (7,12). We therefore expect that imaging the LCX will be similar to that of the LAD and RCA in terms of clear visualization time. Like the RCA, the LCX sits in the atrioventricular groove, so we additionally anticipate that intracoronary motion will be comparable to that of the RCA.

We have not attempted to optimize the size and positioning of the guide catheter, flow rates, or synchronization of the flow rates with actual coronary flow. Additional gains in imaging time and/or decreases in the required saline flow rates may be identified upon further optimization of these parameters. Furthermore, a recent report has demonstrated that nonocclusive purging with isosmolar contrast media can allow high-quality OCT imaging for longer pullback durations (~10 s) (38). The results of this study suggest that the OFDI pullback imaging time may be safely increased and that viscous contrast media may be more efficacious than crystalloids.

Although OFDI is an important advance over OCT, it still has some of the same limitations as the first-generation technology. The most important such limitation is the penetration depth of light, which prohibits visualization of the external elastic lamina in significant plaques. Like OCT, this limitation prevents the use of OFDI for evaluating certain coronary features, such as remodeling. Because this is a fundamental limitation of OFDI and all OCT-related technologies, the best solution to
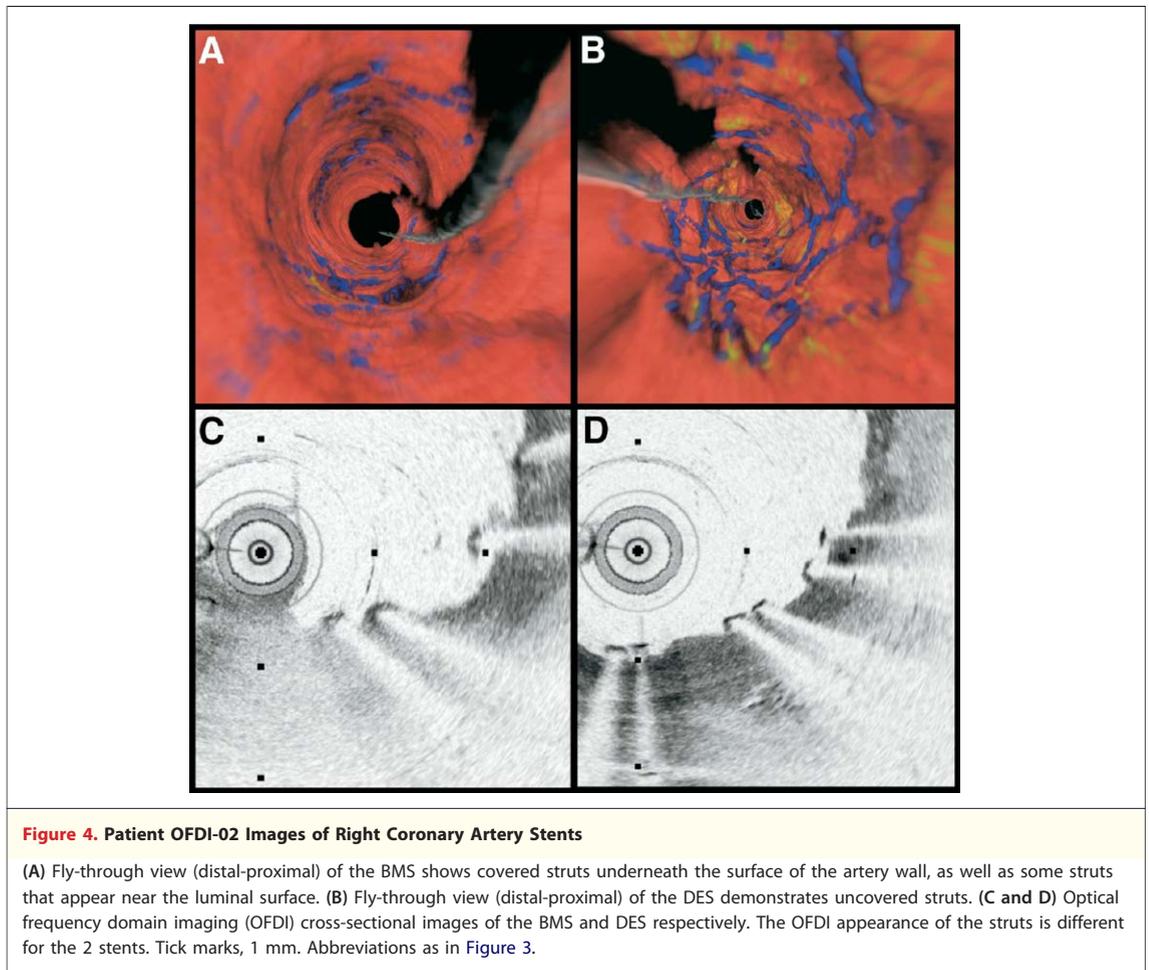
can also be detected by OFDI. Importantly, the ability of OFDI to comprehensively image long coronary segments removes the diagnostic uncertainty that

Figure 4. Patient OFDI-02 Images of Right Coronary Artery Stents

(A) Fly-through view (distal-proximal) of the BMS shows covered struts underneath the surface of the artery wall, as well as some struts that appear near the luminal surface. **(B)** Fly-through view (distal-proximal) of the DES demonstrates uncovered struts. **(C and D)** Optical frequency domain imaging (OFDI) cross-sectional images of the BMS and DES respectively. The OFDI appearance of the struts is different for the 2 stents. Tick marks, 1 mm. Abbreviations as in Figure 3.

this problem may be a hybrid device that combines IVUS and OCT into one instrument. In the interim, before this multimodality device is developed, it will be necessary to use both IVUS and OFDI if visualization of both superficial and deep coronary pathology is required.

There is substantial interest in obtaining longitudinal microscopic information because of recent findings that coronary pathology is highly dependent on shear forces in the direction of blood flow (39). At the maximum pullback velocity of 20 mm/s, our imaging speed of 100 frames/s resulted in an undersampled longitudinal resolution (200 μm). In comparison, for the slowest pullback velocity of 5 mm/s, longitudinal reconstructions were adequately sampled and image quality was comparable with that of the cross-sectional images (Fig. 7). Because both longitudinal information and long imaging lengths are highly desirable, future development of the OFDI method should focus on increasing longitudinal image sampling without sacrificing length. In addition to improving clear-

ance of blood by optimizing saline delivery, these imaging characteristics may be achieved by increasing the frame rate of the OFDI system (40,41).

Although 3D visualization provides a powerful manner to represent the OFDI data, it is currently very time consuming. The volume representations presented here took several hours to create, as many of the segmentation steps were semi-automatic or manual. If 3D visualization becomes important for the use of OFDI in the cardiac catheterization laboratory, additional research must be conducted to develop automatic volume data processing methods that can be completed in real-time during the interventional procedure. The 3D reconstructions also are prone to artifacts caused by linear, rotational, and deformational motion of the artery during the pullback. Electrocardiogram gating (42) or post-acquisition image processing techniques (43) that have been used for IVUS reconstructions can potentially correct these artifacts. Finally, we note that the reproducibility of 3D OFDI volume reconstructions has not yet been established. Stud-
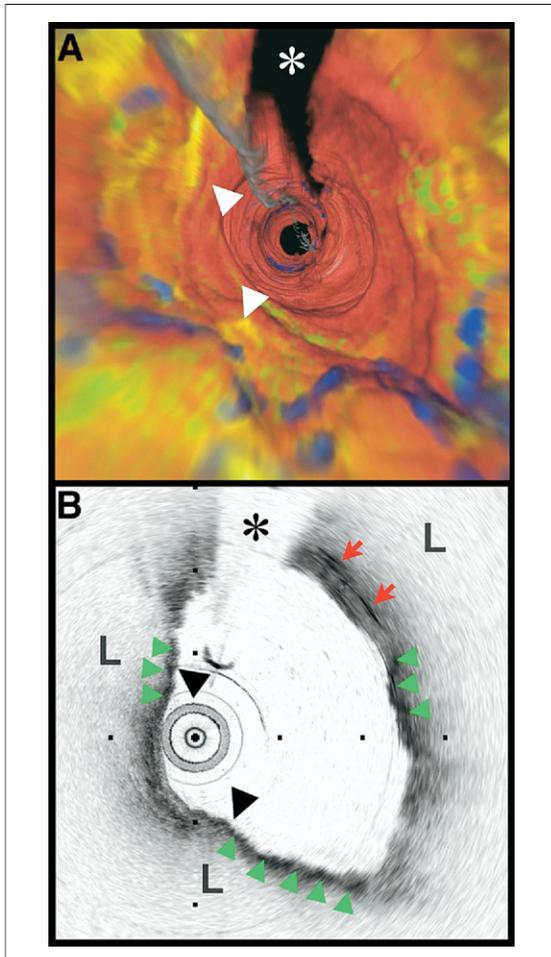
Figure 5. Patient OFDI-02 Images of a Distal Right Coronary Artery Thin-Capped Fibroatheroma

(A) Fly-through view (distal-proximal), demonstrates a circumferential lipid-rich lesion with abundant macrophages, partially covered by the stent. **(B)** An optical frequency domain imaging (OFDI) cross-sectional image obtained at location of **white arrowheads in A** and **dotted line** in Figure 3D, shows a circumferential lipid pool (L). Thin cap sites **(black arrowheads)** can be identified at multiple locations within the cross-sectional image. Macrophages **(green arrowheads)** and cholesterol crystals **(red arrows)** can also be seen. **Tick marks,** 1 mm. *Guide wire artifact.

ies to evaluate the reproducibility of intracoronary OFDI are currently under way.

CONCLUSIONS

We have presented the first human experience with intracoronary OFDI, a second-generation OCT technology. We found that, compared with conventional OCT, the greater speeds of OFDI used in this study enabled comprehensive volumetric microscopy of coronary arteries in living patients after a short and nonocclusive saline flush. The ease of use of this new method along with the wealth of
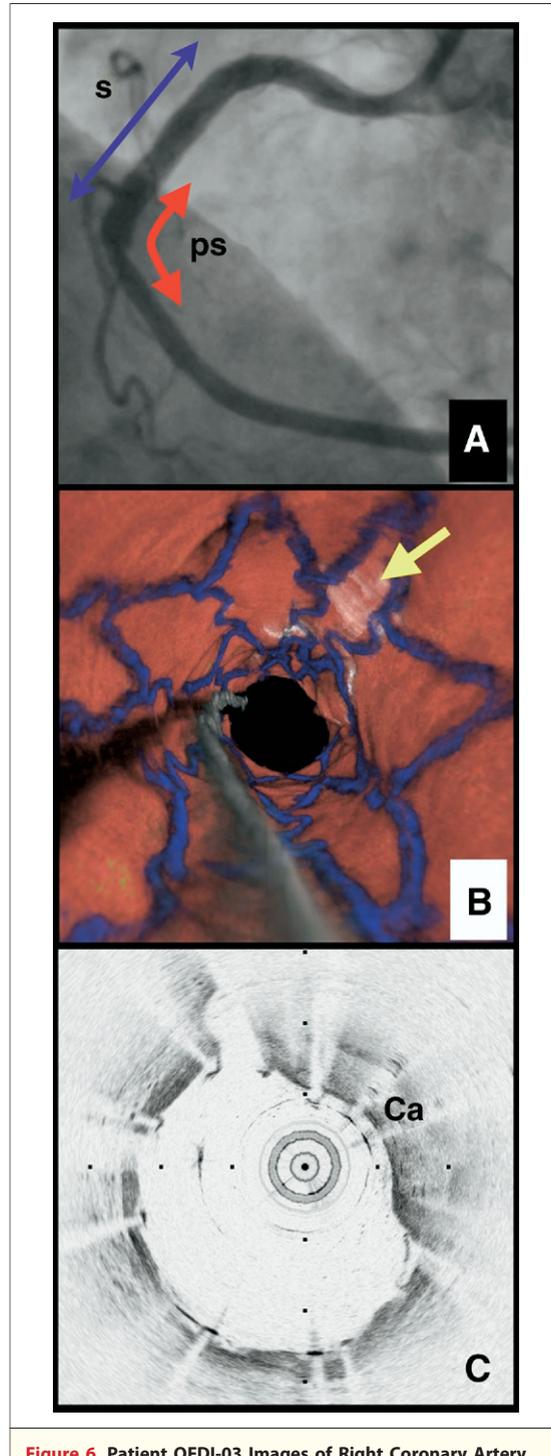

Figure 6. Patient OFDI-03 Images of Right Coronary Artery

(A) A left anterior oblique angiogram after stent deployment shows stent site (s) and 3.0-cm optical frequency domain imaging (OFDI) pullback segment (ps). **(B)** Fly-through view (distal-proximal) demonstrates a calcified lesion underneath the stent **(arrow)**. **(C)** An OFDI cross-sectional image, obtained at location of **yellow arrow in B**, shows a large calcific nodule from 11- to 4-o'clock. **Tick marks,** 1 mm.
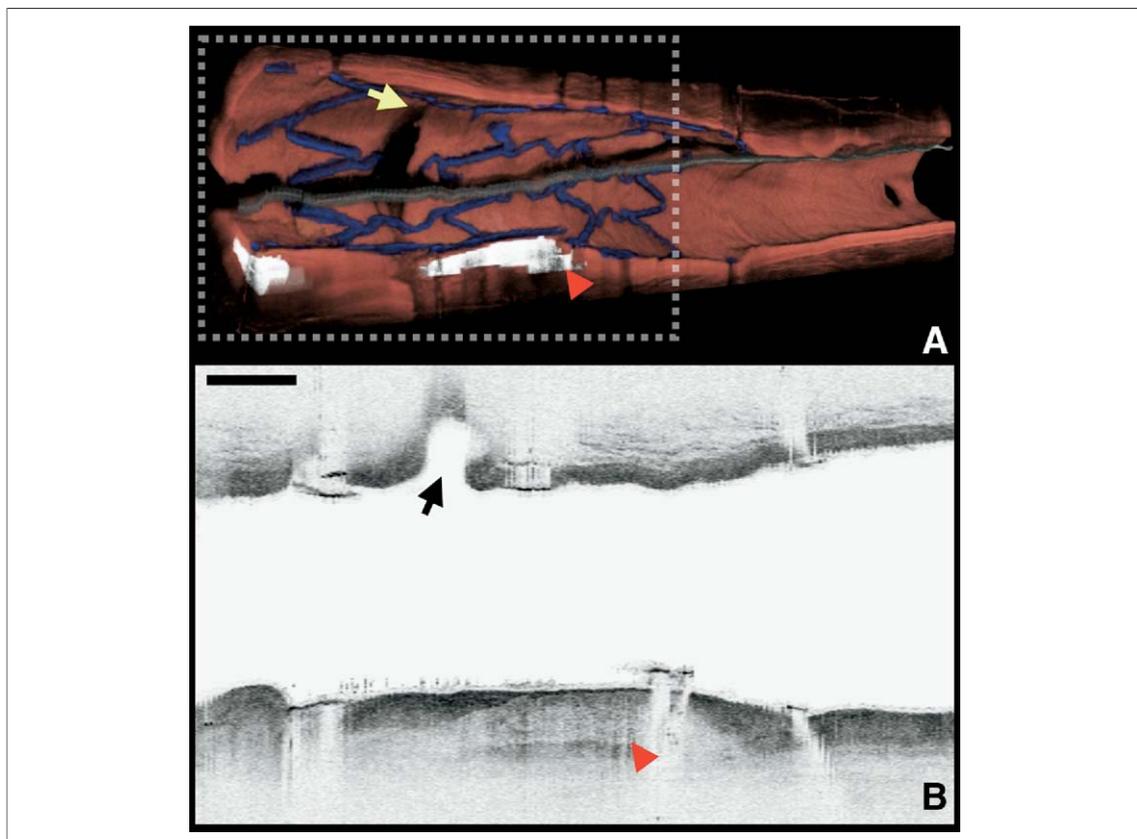
Figure 7. Patient OFDI-03 Images of Right Coronary Artery Stent

(A) Perspective cutaway view of entire 3-dimensional volume rendered optical frequency domain imaging (OFDI) data set (left = proximal; right = distal), demonstrating the stent **(blue)**, a side branch **(yellow arrow)**, and a large calcific nodule **(red arrowhead)**. **(B)** Longitudinal section through a portion of the dataset, corresponding to the **gray dotted rectangle in A**. The side branch **(black arrow)** and calcific nodule **(red arrowhead)** are evident. Scale bar in **B**, 1.0 mm.

information contained in the data bring it closer to becoming a useful imaging technique in cardiac catheterization laboratories.

Acknowledgements

The authors thank Judith Pendleton and Patricia Baum for their invaluable assistance in this study.

REFERENCES

1. Huang D, Swanson EA, Lin CP, et al. Optical coherence tomography. Science 1991;254:1178–81.

2. Brezinski ME, Tearney GJ, Bouma BE, et al. Imaging of coronary artery microstructure (in vitro) with optical coherence tomography. Am J Cardiol 1996;77:92–3.

3. Tearney GJ, Brezinski ME, Boppart SA, et al. Images in cardiovascular medicine. Catheter-based optical imaging of a human coronary artery. Circulation 1996;94:3013.

4. Tearney GJ, Jang IK, Kang DH, et al. Porcine coronary imaging in vivo by optical coherence tomography. Acta Cardiol 2000;55:233–7.

5. Jang IK, Tearney G, Bouma B. Visualization of tissue prolapse between coronary stent struts by optical coherence tomography: comparison with intravascular ultrasound. Circulation 2001;104:2754.

6. Grube E, Gerckens U, Buellesfeld L, Fitzgerald PJ. Images in cardiovascular medicine. Intracoronary imaging with optical coherence tomography: a new high-resolution technology pro-

viding striking visualization in the coronary artery. Circulation 2002;106:2409–10.

7. Jang IK, Bouma BE, Kang DH, et al. Visualization of coronary atherosclerotic plaques in patients using optical coherence tomography: comparison with intravascular ultrasound. J Am Coll Cardiol 2002;39:604–9.

8. Tearney GJ, Yabushita H, Houser SL, et al. Quantification of macrophage content in atherosclerotic plaques by optical coherence tomography. Circulation 2003;107:113–9.

9. MacNeill BD, Jang IK, Bouma BE, et al. Focal and multi-focal plaque macrophage distributions in patients with acute and stable presentations of coronary artery disease. J Am Coll Cardiol 2004;44:972–9.

10. Raffel OC, Tearney GJ, Gauthier DD, Halpern EF, Bouma BE, Jang IK. Relationship between a systemic inflammatory marker, plaque inflammation, and plaque characteristics determined by intravascular optical coherence tomography. Arterioscler Thromb Vasc Biol 2007;27:1820–7.

11. Kume T, Akasaka T, Kawamoto T, et al. Measurement of the thickness of the fibrous cap by optical coherence tomography. Am Heart J 2006;152:755.1–4.

12. Jang IK, Tearney GJ, MacNeill B, et al. In vivo characterization of coronary atherosclerotic plaque by use of optical coherence tomography. Circulation 2005;111:1551–5.

13. Kuo WC, Chou NK, Chou C, et al. Polarization-sensitive optical coherence tomography for imaging human atherosclerosis. Appl Opt 2007;46:2520–7.

14. Giattina SD, Courtney BK, Herz PR, et al. Assessment of coronary plaque collagen with polarization sensitive optical coherence tomography (PS-OCT). Int J Cardiol 2006;107:400–9.

15. Nadkarni SK, Pierce MC, Park BH, et al. Measurement of collagen and smooth muscle cell content in atherosclerotic plaques using polarization-sensitive optical coherence tomography. J Am Coll Cardiol 2007;49:1474–81.

16. Kume T, Akasaka T, Kawamoto T, et al. Assessment of coronary arterial thrombus by optical coherence tomography. Am J Cardiol 2006;97:1713–7.

17. Tearney GJ, Jang IK, Bouma BE. Optical coherence tomography for imaging the vulnerable plaque. J Biomed Opt 2006;11:021002.

18. Tanigawa J, Barlis P, Di Mario C. Intravascular optical coherence tomography: optimization of image acquisition and quantitative assessment of stent strut apposition. EuroIntervention 2007;3:128–36.

19. Bouma BE, Tearney GJ, Yabushita H, et al. Evaluation of intracoronary stenting by intravascular optical coherence tomography. Heart 2003;89:317–20.

20. Raffel OC, Hannan JC, Jang IK. Coronary stent malapposition as a result of a post-stenotic aneurysm detected by optical coherence tomography. J Invasive Cardiol 2006;18:561–2.

21. Sawada T, Shite J, Shinke T, et al. Persistent malapposition after implantation of sirolimus-eluting stent into intramural coronary hematoma: optical coherence tomography observations. Circ J 2006;70:1515–9.

22. Kume T, Akasaka T, Kawamoto T, et al. Visualization of neointima formation by optical coherence tomography. Int Heart J 2005;46:1133–6.

23. Regar E, van Beusekom HM, van der Giessen WJ, Serruys PW. Images in cardiovascular medicine. Optical coherence tomography findings at 5-year follow-up after coronary stent implantation. Circulation 2005;112:e345–6.

24. Regar E, Schaar J, Serruys PW. Images in cardiology. Acute recoil in sirolimus eluting stent: real time, in vivo assessment with optical coherence tomography. Heart 2006;92:123.

25. Takano M, Jang IK, Mizuno K. Neointimal proliferation around malapposed struts of a sirolimus-eluting stent: optical coherence tomography findings. Eur Heart J 2006;27:1763.

26. Barlis P, Tanigawa J, Di Mario C. Coronary bioabsorbable magnesium stent: 15-month intravascular ultrasound and optical coherence tomography findings. Eur Heart J 2007;28:2319.

27. Gupta R, Raffel OC, Jang IK. Severe intimal hyperplasia after sirolimus eluting stent deployment: evaluation by optical coherence tomography. Heart 2007;93:754.

28. Takano M, Inami S, Jang IK, et al. Evaluation by optical coherence tomography of neointimal coverage of sirolimus-eluting stent three months after implantation. Am J Cardiol 2007;99:1033–8.

29. Tanigawa J, Barlis P, Di Mario C. Do unopposed stent struts endothelialize? In vivo demonstration with optical coherence tomography. Heart 2007;93:378.

30. Toutouzas K, Vaina S, Riga MI, Stefanadis C. Evaluation of dissection after coronary stent implantation by intravascular optical coherence tomography. Clin Cardiol 2008. In Press.

31. Yun SH, Tearney GJ, Vakoc BJ, et al. Comprehensive volumetric optical microscopy in vivo. Nat Med 2006;12:1429–33.

32. Yun SH, Tearney GJ, de Boer JF, Iftima N, Bouma BE. High-speed optical frequency-domain imaging. Optics Express 2003;11:2953–63.

33. Eickhoff W, Ulrich R. Optical frequency-domain reflectometry in single-mode fiber. Applied Physics Letters 1981;39:693–5.

34. Rasband WS. ImageJ. Bethesda, MD: U.S. National Institutes of Health, 1997–2005. Available at: http://rsb.info.nih.gov/ij/.

35. Thévenaz P, Ruttimann UE, Unser M. A pyramid approach to subpixel registration based on intensity. IEEE Trans Image Proc 1998;7:27–41.

36. Yabushita H, Bouma BE, Houser SL, et al. Characterization of human atherosclerosis by optical coherence tomography. Circulation 2002;106:1640–5.

37. Finn AV, Joner M, Nakazawa G, et al. Pathological correlates of late drug-eluting stent thrombosis: strut coverage as a marker of endothelialization. Circulation 2007;115:2435–41.

38. Prati F, Cera M, Ramazzotti V, Imola F, Giudice R, Albertucci M. Safety and feasibility of a new non-occlusive technique for facilitated intracoronary optical coherence tomography (OCT) acquisition in various clinical and anatomical scenarios. EuroIntervention 2007;3:365–70.

39. Stone PH, Coskun AU, Kinlay S, et al. Effect of endothelial shear stress on the progression of coronary artery disease, vascular remodeling, and in-stent restenosis in humans: in vivo 6-month follow-up study. Circulation 2003;108:438–44.

40. Oh WY, Yun SH, Tearney GJ, Bouma BE. 115 kHz tuning repetition rate ultrahigh-speed wavelength-swept semiconductor laser. Opt Lett 2005;30:3159–61.

41. Adler DC, Huber R, Fujimoto JG. Phase-sensitive optical coherence tomography at up to 370,000 lines per second using buffered Fourier domain mode-locked lasers. Opt Lett 2007;32:626–8.

42. von Birgelen C, de Vrey EA, Mintz GS, et al. ECG-gated three-dimensional intravascular ultrasound: feasibility and reproducibility of the automated analysis of coronary lumen and atherosclerotic plaque dimensions in humans. Circulation 1997;96:2944–52.

43. Nadkarni SK, Boughner D, Fenster A. Image-based cardiac gating for three-dimensional intravascular ultrasound imaging. Ultrasound Med Biol 2005;31:53–63.

Key Words: intravascular imaging ▪ coronary imaging ▪ optical coherence tomography ▪ stents.